Low-frequency Signal Generation in Space Based on the High-frequency Electric Antenna Array and Doppler effect

Anjing Cui
School of Electronic, Electrical and Communication Engineering, University of Chinese Academy of Sciences

Daojing Li (lidj@mail.ie.ac.cn)
National Key Lab of Microwave Imaging Technology, Aerospace Information Research Institute, Chinese Academy of Sciences

Jiang Wu
School of Electronic, Electrical and Communication Engineering, University of Chinese Academy of Sciences

Jinghan Gao
School of Electronic, Electrical and Communication Engineering, University of Chinese Academy of Sciences

Kai Zhou
School of Electronic, Electrical and Communication Engineering, University of Chinese Academy of Sciences

Chufeng Hu
National Key Laboratory of Science and Technology on Unmanned Aerial Vehicle, Northwestern Polytechnical University

Shumei Wu
National Key Lab of Microwave Imaging Technology, Aerospace Information Research Institute, Chinese Academy of Sciences

Article

Keywords:

Posted Date: July 25th, 2022

DOI: https://doi.org/10.21203/rs.3.rs-1852505/v1

Abstract

Low-frequency signals can be used in target detection and geological exploration, but the large antenna sizes limit their applications. Hence, it is significant to investigate the low-frequency signal generation method based on antennas with appropriate sizes. Different from mechanical antenna methods, previous work of this paper proposes a novel low-frequency signal generation method in space on the basis of Doppler effect, and designs the high-frequency electric antenna staggered array and timing sequency of the periodic pulse train signal. In this paper, 8-element short-array and 64-element long-array experimental prototypes are proposed, and the 121.35 MHz signal is composed of 156 MHz radiating element signals. Experimental results show that the measured composite signal spectrums are similar to the simulations and physically verify the feasibility of the low-frequency signal generation method based on the high-frequency electric antenna array, which is valuable in the area of low-frequency signal generation with small antennas.

Introduction

In order to radiate electromagnetic waves efficiently, size of the traditional antenna must reach 1/4 wavelength of the signal, which limits the application of low-frequency (LF) electromagnetic waves. Research of the LF/ very-low-frequency (VLF) signal generation method based on high-frequency antennas with appropriate sizes is valuable in target detection[1,2] and geological exploration[3,4].

With acoustic excitation or mechanical drive mechanical antennas adopted, Reference 5,6,7 studies the LF signal generation meth-od based on the principle of magnetoelectric coupling. The method decreases the size of the LF signal antenna and enables low-frequency wireless communication systems and radars to be applied to mobile platforms. Compared with the mechanical antenna method, previous work of this paper uses electric antennas and proposes a novel LF signal generation method in space based on the high-frequency antenna array.

The LF signal generation method based on the antenna array is proposed in Reference 8, and the simulation of 400 MHz signal, which is composed of 1 GHz radiating element signals (RE signal) and the 100 m array, is presented. The method generates signals with different frequency in various directions and makes it possible to detect targets with the multiband antenna array[9]. In further research, Reference 10 combines the staggered array and the periodic pulse train signal, proposes the method of generating VLF signals and gives simulations of 10 kHz signals generated by 100 MHz RE signals. Other than the transient electromagnetic scattering method[11], this method provides a new idea of geological exploration with movable platforms.

The principle, method and characteristics of the method are as follows.

- Principle of frequency conversion: according to Doppler effect[12], when the radar moves away from the target at the velocity close to light speed and the signal is received in the stationary target area,

the frequency of the receiving signal decreases and the pulse width broadens.

- The physical method: the array structure is adopted to emulate the receiving signal when the radar leaves at near-light speed, the large array structure makes near-light motion of the radar possible, and the LF/VLF signal is composed in space.
- Improvement of composite signal performance: multiple arrays are used to reduce the spacing of radiating elements, the RE signal is designed as periodic pulse train signal, and the rest period of the signal is filled by the broadened pulse, which contribute to generation of LF /VLF signal and reduce the impact of harmonics.
- The nonlinear and wideband system: considering the frequency and pulse width conversion, the process of LF/VLF signal generation is non-linear and wideband.

Reference 8,10 complete the theoretical analysis and computer simulation, and the validity of the methods need to be proved through physical experiments. As a continuation of the work in Reference 10, on the basis of the staggered array structure and the periodic pulse train signal, the experimental prototype and scheme of generating the 121.35 MHz signal with 156 MHz RE signals are designed in this paper, and the 8-element short-array and 64-element long-array experiments are introduced. The experimental results verify the feasibility of the proposed method physically and are likely to promote the development of LF signal generation method based on small antennas.

Methods

Principle, method and previous work

According to Doppler effect, when the radar moves away from the stationary receiving antenna, the frequency of the receiving signal decreases and the pulse broadens. Equations of frequency f_r, doppler frequency f_d and pulse width $\tau_r$of the receiving signal are illustrated as follows.

$$f_r = \sqrt{(c-v)/(c+v)}f_0$$

1

$$f_d = f_r - f_0 = \left[\sqrt{(c-v)/(c+v)} - 1\right] f_0$$

2

$$\tau_r = \sqrt{(c+v)/(c-v)}\tau_0$$

3

where f_0 and τ_0 are frequency and pulse width of the radar signal, and are velocities of the radar and light.

Reference 8 enables the composite signal of the antenna array to be equivalent to the receiving signal when the radar leaves through setting waveform, phase and time series of RE signals. Figure 1(a) shows the discrete process of the radar moving and emitting signal. The initial distance between the receiving antenna and the radar is R_0, the radar moves away from the receiving antenna at the speed of , and the process is decomposed by time interval Δt. Figure 1(b) introduces the equivalent antenna array: the radiating element spacing is $v\Delta t$, radiating elements from the near end to the far end of the array transmit signals at time interval Δt sequentially, and initial phases of RE signals are set specifically. With time interval Δtsmaller than carrier period of RE signal, the composite signal in space is modulated multiple times in a carrier period, thus the LF signal is generated.

On the basis of Reference 8, the staggered array and periodic pulse train signal are proposed in Reference 10.

Structure of the staggered array is shown in Fig. 1(c), where λ_0 is the carrier wavelength of the RE signal, and is radiating element spacing. Compared with the traditional antenna array, which limits radiating element spacing with half-wavelength of the carrier, the staggered array reduces radiating element spacing through arranging multiple arrays. When radiating elements are small enough, multiple arrays can form one antenna array. Through shortening element spacing, the staggered array reduces the time interval and improves the performance of the composite signal.

Waveform of the periodic pulse train signal with 50% duty cycle is presented in Fig. 1(d), where T_0 and are period and broadcast period of the signal. Bandwidth of the signal is determined by the pulse width, and the initial phase of each pulse is set according to Doppler effect. Multiple carrier periods are included in T_0, and the signals in different broadcast period are the same. RE signal is the periodic pulse train signal, the resting period of the signal can be filled by the broadened pulse generated by the array, and the pulse width of the composite signal can be increased through increasing the number of periods of the signal, which lays foundation for generation of VLF signals.

As previous work of this paper, Reference 8,10 analyze and derive the principle and method of LF and VLF signal generation under conditions of the antenna array and the staggered array respectively, and the corresponding simulations are completed.

When the receiving antenna and the array form a 45° angle, 400 MHz LF composite signal based on 105 m antenna array and phase-modulated RE signals at 1 GHz carrier frequency is simulated in Reference 8, 10 kHz VLF composite signal generated by 120 m staggered array and RE signals at 100 MHz carrier frequency is simulated in Reference 10. Parameters, such as peak sidelobe ratio (PSLR) and integral sidelobe ratio (ISLR)[13], are applied to evaluate the performance of the composite signal.

The simulation parameters in Reference 8,10 are listed in Table 1, and simulation results are shown in Fig. 2. It is necessary to explain that the emission signal in figure is product of one RE signal and the number of radiating elements. Due to the same spectrum of RE signals, the emission signal spectrum can indicate the energy distribution of all RE signals in each frequency component. Random phase composite signal is generated by RE signals with random phase, and its comparison with the composite signal illustrates the necessity of RE signal phase setting.

System composition and equipment parameters

The scheme is divided into two parts, including 8-element short-array experiment and 64-element long-array experiment.

Radiating elements are fed by the 8-channel digital module directly in the 8-element short-array experiment. As displayed in Fig. 3(a), 1×8 power splitters, cables and the 8-channel digital module are combined to feed the radiating elements in the 64-element long-array experiment, and the array structure refers to the staggered array structure in Fig. 1(c).

The RE signals are generated by the digital module, which bases on an 8-channel Digital Analogue Converter (DAC). The clock frequency of the 14-bit DAC is 1 GHz, the signal generation is controlled by the server, the waveform is determined by the data stored in Random Access Memory (RAM), and channels of the digital module work independently and circularly. Photos of the digital module, the server and waveform of the signal output are presented in Fig. 3(b)-(c).

TX170 whip antenna is selected to be the radiating element. In the 8-element short-array experiment, radiating elements are connected to the digital module by cables. In the 64-element long-array experiment, radiating elements are connected to the 1×8 power splitter by cables, and length of cables connecting to the same power splitter vary. In the direction along the array, a log-periodic antenna is set to receive the composite signal, and the signal is analyzed by a spectrometer. Parameters of the experimental equipment and the short/long-array experiment based on the 8-channel digital module are listed in Table 2, where the equivalent radar speed and the frequency of the composite signal are determined by the parameters of unequal-length cables.

Design and test results of unequal-length cables

Radiating elements in the antenna array emit periodic pulse train signals, and formulae of the signals are illustrated in Reference 10. The delay and phase difference of signals emitted by adjacent radiating elements are as follows.

$$\Delta t = d / v$$

4

$$\Delta\varphi = \varphi_{n+1} - \varphi_n = 2\pi f_0 \sqrt{1 - (v/c)^2} d/v$$

5

where is the number of radiating elements, and $n = 0, 1, \cdots, N-1$ is the radiating element serial number.

In order to simplify the experimental prototype and feed 64 radiating elements with the 8-channel digital module at the same time, radiating elements are divided into groups, with 8 radiating elements in a group. On the foundation that each channel of the digital module generates one RE signal, whose phase and delay are certain, unequal-length cables are applied to generate delay and phase changes for other RE signals in the group[14,15].

Supposing that the length difference between unequal-length cables connected to adjacent radiating elements is l_0, then the delay and phase change generated are

$$T_D = l_0 \sqrt{\varepsilon_r}/c$$

6

$$\Delta\varphi = \beta l_0$$

7

where ε_r is relative dielectric constant of the medium and β is phase constant of the cable. Comparing Eq. (4) to (7), equations can be formed. The l_0, which determines the delay and phase change of the RE signal, can be calculated.

Through calculation and simulation, within the constraints of the experimental conditions, it can be found that the composite signal has good performance when l_0= 0.683 m, the equivalent radar velocity is $0.246c$, and frequency of the composite signal is 121.35 MHz.

To make it convenient to connect power splitters and radiating elements, the shortest length of unequal-length cable is 0.20 m, and parameters of unequal-length cables are shown in Table 3.

Table 3
Parameters of unequal-length cables

Cable number	Length /m	Attenuation /dB	Relative phase /rad	Delay /ns
1	0.20	0.0735	0	0.95238
2	0.88	0.3232	-3.1093	4.1905
3	1.57	0.5767	0.1113	7.4762
4	2.25	0.8264	-2.9980	10.714
5	2.94	1.0799	0.2226	14.000
6	3.62	1.3296	-2.8867	17.238
7	4.30	1.5794	0.2872	20.476
8	4.99	1.8328	-2.7754	23.762

Power splitters and the digital module are connected with 8 m cables, and radiating elements are connected to power splitters with unequal-length cables. With the experiment set up in spatial, time and frequency domain, the time and phase accuracy of RE signals have a significant influence on the experimental result.

In order to test the transmission delay of cables and power splitters, 2 channels of the digital module are set to emit signals, with channel 1 and 2 connected to the oscilloscope and the device to be tested separately. The result is displayed in Table 4. According to the test, the average delay difference between unequal-length cables is 3.258 ns. Compared with 3.252 ns ideal delay difference, the average delay error is less than 0.01 ns (corresponding to 2.1 mm cable length error), and variation range of the delay error is within ± 0.3ns. Thus, the transmission delay error of cables and power splitters has little influence on the composite signal.

Table 4
Transmission delay performance test

Device tested (Channel 0)	Delay relative to channel 1 / ns	Transmission delay/ ns	Delay difference/ ns
without cable	13.333	0	/
8 m cable	24.778	11.445	/
8 m cable, power splitter and 0.20 m cable	27.079	13.746	/
8 m cable, power splitter and 0.88 m cable	30.225	16.892	3.146
8 m cable, power splitter and 1.57 m cable	33.371	20.038	3.146
8 m cable, power splitter and 2.25 m cable	36.742	23.409	3.371
8 m cable, power splitter and 2.94 m cable	40.000	26.667	3.258
8 m cable, power splitter and 3.62 m cable	43.371	30.038	3.371
8 m cable, power splitter and 4.30 m cable	46.405	33.072	3.034
8 m cable, power splitter and 4.99 m cable	49.888	36.555	3.483

Simulation and analysis

According to the experimental parameters in Table 2 and Table 3, spectrums of the 121.35 MHz composite signals based on the 8-element short array and 64-element long array in the direction along the array are simulated respectively.

Simulation and analysis in the ideal case

The simulated composite signal spectrums based on the 8-element short array and 64-element long array in the ideal case are shown in Fig. 4(a) and Fig. 4(c). Spectrum comparisons of the emission signals, the composite signals and random phase composite signals are presented in Fig. 4(b) and Fig. 4(d), and comparisons indicate that phase and delay of RE signals have significance in the LF signal generation process.

In the short-array experiment, with the short array, few radiating elements and close distance between the receiving antenna and the array leading to increase of the carrier and harmonic component, the simulation results show that the composite signal based on the short array can generate apparent low-frequency component. Meanwhile, PSLR of the composite signal based on the long array is -14.8182 dB,

ISLR is -6.9479 dB (83.20%), and the energy utilization ratio of the composite signal to the emission signal is about 79.97%.

Simulation and analysis of error influence

Random errors and system errors exist in short/long-array experiment. Simulation and analysis indicate that ± 0.5 cm spacing error, ± 1 ns delay error and ± 10° phase error of RE signals, and ± 0.05 normalization amplitude error (corresponding to -0.45dB to 0.42dB) have little influence on the composite signal, when the errors above are random errors and distribute uniformly. In the process of the experiment, parameter errors of the prototype can be controlled within the ranges above. Therefore, influence of system errors is simulated and analyzed in this section.

The clock frequency and time resolution of the digital module is 1 GHz and 1 ns, and delay system error may be caused, which is less than 1 ns and exists in the short/long-array experiment. In the long-array experiment, power splitters and radiating elements are connected by cables, and they can lead to the phase system error[16,17]. Due to the limitation of the experimental environment and power of the RE signals, the receiving antenna is close to the antenna array, which makes the amplitudes of received RE signals differ, and the performance of the composite signal is affected.

The simulated composite signal spectrums based on the short array and long array under the influence of system errors are shown in Fig. 4(e) and Fig. 4(f). Figure 4(e) presents the composite signal spectrum based on the short array when the receiving antenna is 6 m away from the array and 0.1 ns delay system error exists. Figure 4 (f) shows the composite signal spectrum based on the long array when the receiving antenna is 20 m away from the array with 0.1 ns delay system error and 30° phase system error existing. After accumulation, the delay system error can reach 0.7 ns. Under the condition that system errors exist, the simulation results indicate that delay system error has little effect on the composite signal of the short array, while the simultaneous delay error and phase system error lead to the increase of carrier component of the composite signal based on the long array.

The phase of the RE signal is designed according to the parameters when the receiving antenna is set in the direction along the array. When the receiving antenna deviates from the direction along the array, the composite signal frequency is higher than the designed frequency. When the receiving antenna is located in the normal direction of the array, the peak frequency of the composite signal is the same as the carrier frequency of RE signals. In the condition that the receiving antenna is 22 m/24 m away from the near end of the array and 38°/51° deviates from the array direction, and influenced by system errors mentioned in Fig. 4(f), the simulated composite signal spectrums based on the long array are shown in Fig. 4(g) and Fig. 4(h).

Results

8-element short-array experiment

The 8-element short-array experiment is completed in the anechoic chamber of Northwestern Polytechnical University and the rooftop of Aerospace Information Research Institute. Considering influence of the experimental background, the anechoic chamber can provide ideal experimental environment, but the outdoor experiment also works if no interfering frequency exists near the composite signal frequency. Figure 5(a)-(b) exhibit photos of the experiment.

All radiating elements of the short array are fed by the digital module, and the outdoor experimental result is shown in Fig. 5(d). The experiment result presents that 121.35 MHz composite signal is generated successfully, and the spectrum measured is similar to the simulation.

Unequal-length cable test with 1 DAC channel and 8 radiating elements

In the long-array experiment, 64 radiating elements are fed by the 8-channel digital module, power splitters and unequal-length cables. The result of the unequal-length cable test with 1 DAC channel and 8 radiating elements is displayed in Fig. 6(b). Comparing Fig. 5(d) and Fig. 6(b), the feasibility of reducing DAC channels with power splitters and cables is verified.

64-channel long-array experiment

The 64-channel long-array experiments are carried out in a square, and experimental photos are presented in Fig. 6(c)-(d).

The composite signal spectrums measured in different conditions are demonstrated in Fig. 6(e)-(h), and experimental conditions are listed in as follows.

- Condition of experiment 1: RE signal with random initial phase, the receiving antenna 21 m away from the near end of the array and in the array direction
- Condition of experiment 2: RE signal with designed initial phase, the receiving antenna 21 m away from the near end of the array and in the array direction
- Condition of experiment 3: RE signal with designed initial phase, the receiving antenna 22 m away from the near end of the array and 38° deviates from the array direction
- Condition of experiment 4: RE signal with designed initial phase, the receiving antenna 24 m away from the near end of the array and 51° deviates from the array direction

Comparing the experiment results and simulations in Fig. 6 and Fig. 4, the feasibility of the LF signal generation method based on the high-frequency electric antenna array proposed in Reference 8,10 is verified. The frequency and power of the composite signal in different directions vary. In the array direction, the receiving antenna can obtain the composite signal with lowest frequency. When the receiving antenna 90° deviates from the array direction, the main frequency of the composite signal is equal to the carrier frequency of RE signals.

Discussion

With experimental results similar to simulations, the effectiveness of the LF signal generation method based on the high-frequency electric antenna array is verified. The experimental results indicate that frequencies of the composite signals generated through the method proposed in this paper differ. The phenomena conform to the theoretical analysis. The LF signal generation method proposed may be applied to multiband detection of the target. Limited by the experimental conditions, the long-array prototype is simplified with power splitters and cables, but the performance degradation of the LF signal generated is caused at the same time. The problem can be solved by introducing phase shifters[18,19] into the prototype.

Omnidirectional antennas are used in simulation and experiments in this paper. The aim of using multiple radiating elements is to compose LF/VLF signals, and the array gain is not taken into consideration. In further research, the beam width of the antenna array can be reduced and the gain can be improved through constructing subarrays with radiating elements in the pitch direction.

The LF/VLF signal generation principle in space, which combines Doppler effect and the array structure, is clear, and the method has been preliminarily verified through physical experiments. With the aim to improve the gain of antennas and increase the detection range, relevant research will continue on the basis of the antenna array length at the order of 100 m.

Declarations

Data availability

All data generated or analyzed during this study are included in this published article and its supplementary information files.

Competing interests

The authors declare no competing interests.

Acknowledgements

This work is supported by Science and Technology Project of Aerospace Information Research Institute, Chinese Academy of Sciences under Grant Y910340Z2F.

Author contributions

A. C. and D. L. proposed the original idea, completed simulations, designed and participated in the experiments, prepared the manuscript and discussed the results; J. W., J. G. and K. Z. participated in the experiments in Aerospace Information Research Institute; C. H. provided equipment and participated in the experiments in Northwestern Polytechnical University; S. W. provided the digital module.

References

1. Kuschel, H., Heckenbach, J. & Müller, St., Appel, R. Countering stealth with passive, multi-static, low frequency radars. IEEE Aero. El. Sys. Mag. **25**, 11–17, doi:10.1109/MAES.2010.5592986 (2010).
2. Wang, X., Gong, H., Zhang, S., Liu, Y., Yang, R. & Liu, C. Efficient RCS Computation Over a Broad Frequency Band Using Subdomain MoM and Chebyshev Approximation Technique. IEEE Access **8**, 33522–33531, doi:10.1109/access.2020.2974070 (2020).
3. Zhou, Z. & Huang, X. Penetration Performance Analysis of VHF/UHF Ultra-Wideband Synthetic Aperture Radar. J. Syst. Eng. Electron. **25**, 1336–1340, doi:10.3321/j.issn:1001-506X.2003.11.007 (2003).
4. Lu, J., Zhuo, X., Liu, Y., Zhao, G. & Di, Q. The Extremely Low Frequency Engineering Project for Underground Exploration. Engineering **10**, 13–20, doi:10.1016/j.eng.2021.12.003 (2022).
5. Nan, T. et al. Acoustically actuated ultra-compact NEMS magnetoelectric antennas. Nat. Commun. **8**, 296, doi:10.1038/s41467-017-00343-8 (2017).
6. Ren, W., Chen, S., Gao, Y., Li, J. & Peng, C. Progress and technical framework of the BAW mediated magnetoelectric antenna. Chinese J. Radio SCI. **36**, 491–497 + 510, doi:10.13443/j.cjors.2020042202 (2021).
7. Barani, N., Kashanianfard, M. & Sarabandi, K. A Mechanical Antenna With Frequency Multiplication and Phase Modulation Capability. IEEE T. Antenn. Propag. **69**, 3726–3739, doi:10.1109/tap.2020.3044385 (2021).
8. Cui, A., Li, D., Zhou, K., Wang, Y. & Hong, J. On method of composing low frequency signals based on array structures. Acta Phys. Sin-ch Ed. **69**, doi:10.7498/aps.69.20200501 (2020).
9. Rao, P. H., Sujitha, S. & Selvan, K. T. A Multiband, Mutipolarization Shared-Aperture Antenna: Design and evaluation. IEEE Antenn. Propag. M. **59**, 26–37, doi:10.1109/map.2017.2706654 (2017).
10. Cui, A., Li, D., Zhang, S., Wang, Y. & Hong, J. Research on the Method of Composing Very Low Frequency Signals Based on the Staggered Array. J. Radars **9**, 925–938, doi:10.12000/JR20082 (2020).
11. Kuo, C. H. & Moghaddam, M. Electromagnetic Scattering from a Buried Cylinder in Layered Media With Rough Interfaces. IEEE T. Antenn. Propag. **54**, 2392–2401, doi:10.1109/tap.2006.879208 (2006).
12. Walker, J., Halliday, D. & Resnick, R. Relativity in *Fundamentals of Physics* (ed. Walker, J.) 1135–1137 (Wiley, 2014).
13. Wei, Z. Satellite-based SAR Image Quality Assessment Metrics in *Synthetic Aperture Radar Satellite* (ed. Guo, H.) 204–206 (China Science Publishing & Media Ltd., 2001).
14. Skolnik, M. Phased Array Radar Antennas in *Radar Handbook* (ed. Skolnik, M.) 13.1-13.74 (McGraw-Hill, 2008).
15. Czuba, K. & Sikora, D. in 18-th International Conference on Microwaves, Radar and Wireless Communications 1–3 (2010).

16. Ge, Y., Huang, H. & Yuan, H. Phase characteristics of coaxial cable caused by temperature and mechanical bending. J. Thz. Sci. Electron. Inform. Technol. **17**, 621–626, doi:10.11805/TKYDA201904.0621 (2019).
17. Lampe, R. W. Compensation of phase errors due to coaxial cable flexure in near-field measurements. in International Symposium on Antennas and Propagation Society, Merging Technologies for the 90's 1322–1324 (1990).
18. Chen, X., Yang, L., Fu, G. & Gong, S. Effect analysis of phase quantization error of phase shifter on phase center of phased array antenna. Chinese J. Radio Sci. **30**, 1175–1181, doi:10.13443/j.cjors.2015013102 (2015).
19. Zhang, G. Phase Feed Principle of Phased Array Antenna in *Principle of phased array radar* (ed. Wang, X.) 108–113 (National Defense Industry Press, 2009).

Tables

Table 1 and 2 is available in the Supplementary Files section.

Figures

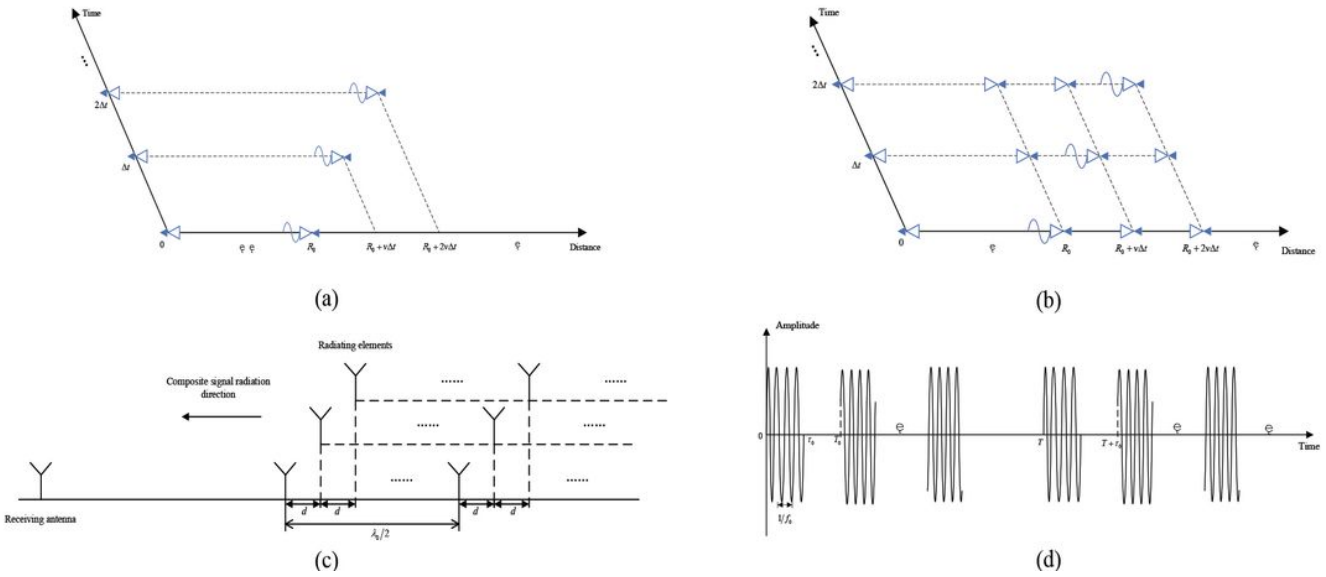

Figure 1

Schematic diagram of the discrete process of radar motion, the equivalent radar motion generated by the antenna array, the staggered array structure and the RE signal. (a) Schematic diagram of the decomposed process of radar motion; (b) Schematic diagram of the equivalent radar motion generated by the antenna array. (c) Schematic diagram of the staggered array structure. (d) Schematic diagram of the RE signal.

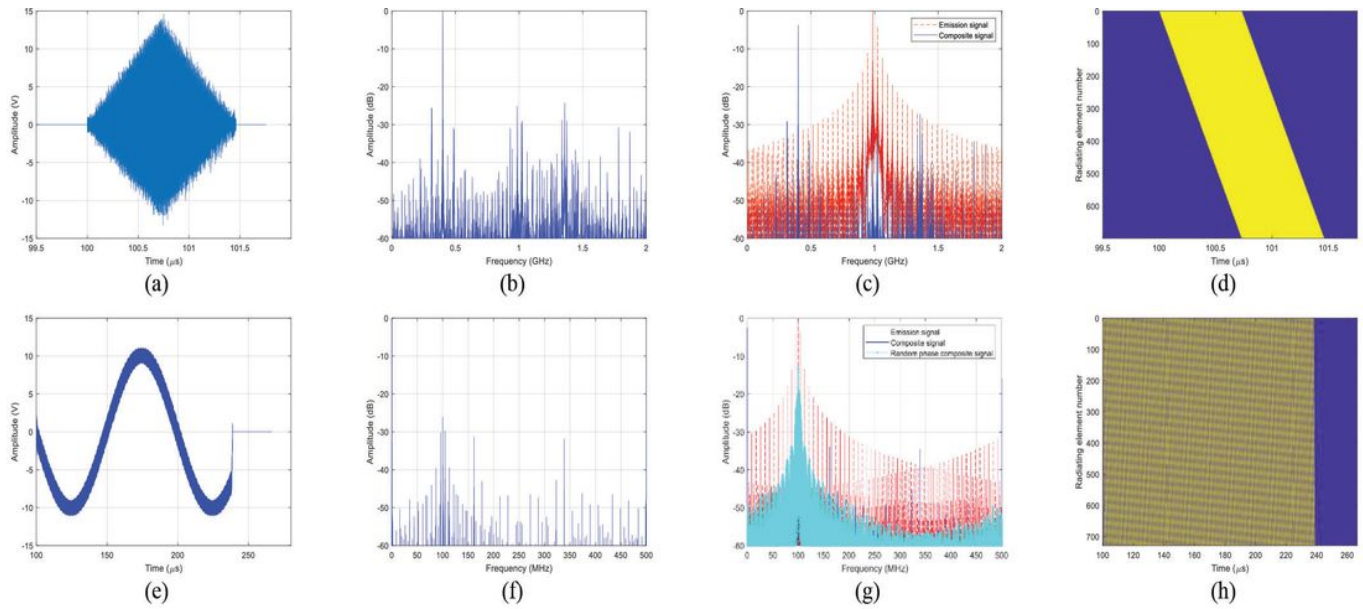

Figure 2

400 MHz LF signal simulation based on the array structure and 10 kHz VLF signal simulation based on the staggered array. (a) Waveform of the 400 MHz composite signal. (b) Spectrum of the 400 MHz composite signal. (c) Spectrum comparison of the emission signal and the 400 MHz composite signal. (d) Envelopes of 1 GHz RE signals. (e) Waveform of the 10 kHz composite signal. (f) Spectrum of the 10 kHz composite signal. (g) Spectrum comparison of the emission signal, the 10 kHz composite signal and the random phase composite signal. (h) Envelopes of 100 MHz RE signals

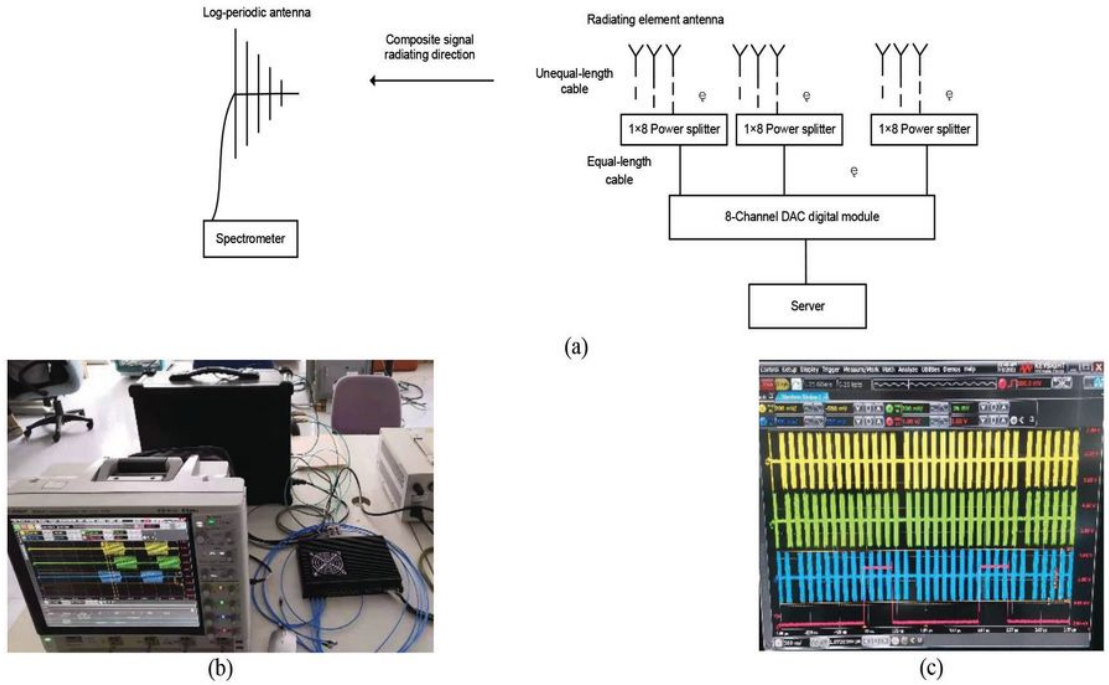

Figure 3

Block diagram of the 64-element long-array experiment and photos of the digital module, the server and waveform of the signal output. (a) Block diagram of the 64-element long-array experiment. (b) Photo of the digital module and the server. (c) Photo of waveform of the signal output

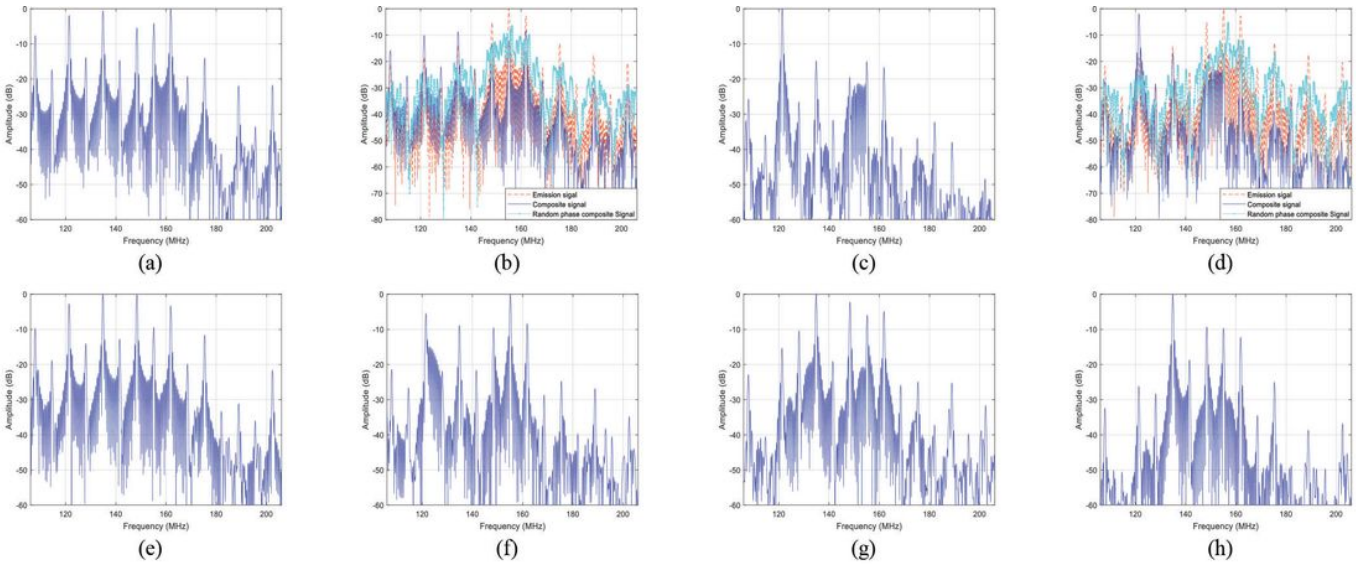

Figure 4

Spectrum simulation and system error analysis of short/long-array experiment. (a) Spectrum of the composite signal in the short-array experiment. (b) Spectrum comparison of the emission signal, the composite signal and the random phase composite signal in the short-array experiment. (c) Spectrum of the composite signal in the long-array experiment. (b) Spectrum comparison of the emission signal, the composite signal and the random phase composite signal in the long-array experiment. (e) Spectrum of the composite signal in the short-array experiment under the influence of system errors. (f) Spectrum of the composite signal in the long-array experiment under the influence of system errors. (g) Composite signal spectrum in the long-array experiment when the receiving antenna 38° deviates from the array direction. (h) Composite signal spectrum in the long-array experiment when the receiving antenna 51° deviates from the array direction.

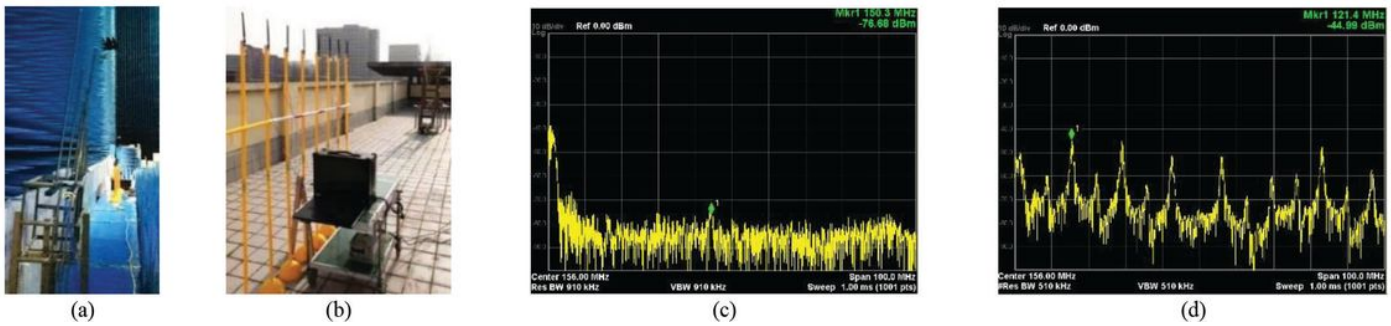

Figure 5

Photos of the 8-element short-array experiments, experimental background and the results of the experiment. (a) Photo of the experiment in the anechoic chamber. (b) Photo of the experiment on the rooftop. (c) Experimental background. (d) Spectrum of the composite signal.

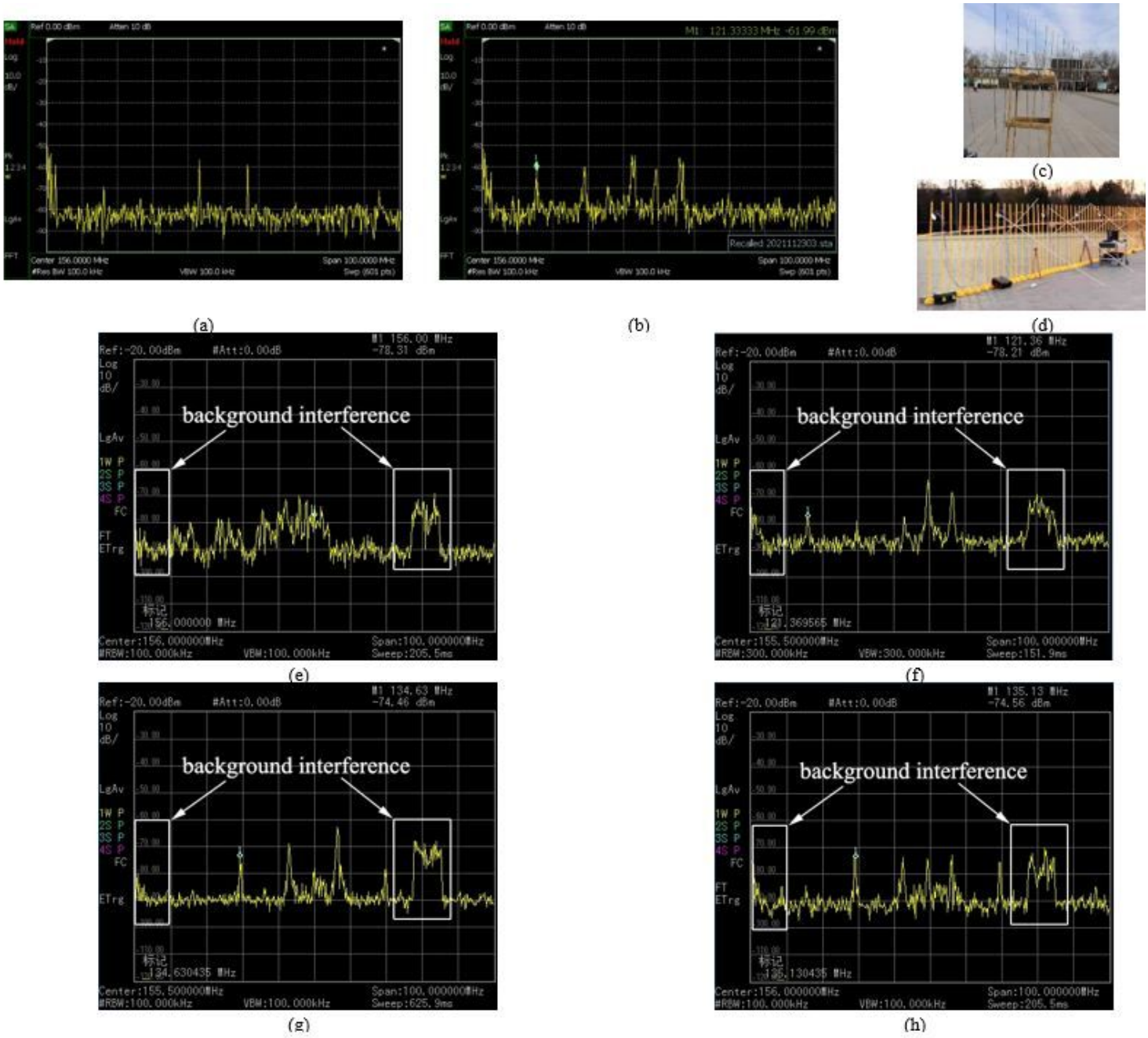

Figure 6

Experiment results of the unequal-length cable test, photos and results of the long-array experiments. (a) Experimental background of the unequal-length cable test. (b) Composite signal spectrum of the unequal-length cable test. (c) The receiving antenna of the long-array experiment. (d) The long array of the long-array experiment. (e) Spectrum of the composite signal in experiment 1. (f) Spectrum of the composite

signal in experiment 2. (g) Spectrum of the composite signal in experiment 3. (h) Spectrum of the composite signal in experiment 4.

Supplementary Files

This is a list of supplementary files associated with this preprint. Click to download.

- Table12.docx